Magnetic ordering in U_2Pd_2In and U_2Pd_2Sn

A. Purwanto* and R. A. Robinson
Los Alamos Neutron Scattering Center, Los Alamos National Laboratory, New Mexico 87545

L. Havela, V. Sechovský, and P. Svoboda
Department of Metal Physics, Charles University, CZ-12116 Prague 2, The Czech Republic

H. Nakotte, K. Prokeš, and F. R. de Boer
Van der Waals-Zeeman Laboratory, University of Amsterdam, 1018 XE Amsterdam, The Netherlands

A. Seret, J. M. Winand, J. Rebizant, and J. C. Spirlet
European Commission, Joint Research Centre, Institute for Transuranium Elements, Post Box 2340, 76125 Karlsruhe, Germany
(Received 12 May 1994)

The tetragonal intermetallic compounds U_2Pd_2In and U_2Pd_2Sn have been studied by means of magnetic susceptibility, magnetization, specific heat, electrical resistivity, and x-ray- and neutron-diffraction techniques. The compounds order antiferromagnetically at 36 and 41 K, respectively, and have enhanced electronic specific-heat coefficients γ of 393 and 203 mJ/mol f.u. K^2, respectively. At low temperature, the nearest-neighbor U-U spacing is along the c axis in both compounds, though in U_2Pd_2Sn the in-plane U-U distance is shorter at room temperature. This crossover is due to motion of the U atoms within the cell rather than anisotropy of the thermal contraction. It is now well established in several classes of (1:1:1) uranium ternary intermetallic compounds that the strong magnetic anisotropy is correlated with the direction of nearest-neighbor U-U links; the moments are almost invariably oriented perpendicular to such links. This is also the case for U_2Pd_2In and U_2Pd_2Sn, where the moments lie in the tetragonal basal plane in a canted arrangement along [110] and [1$\bar{1}$0] directions. Of four such Shubnikov subgroups of $P4/mbm$, one is clearly preferred by the data. At 10 K, the magnetic moments extracted are $(1.6\pm0.2)\mu_B$ and $(2.0\pm0.1)\mu_B$ per U atom in U_2Pd_2In and U_2Pd_2Sn, respectively.

I. INTRODUCTION

Several groups of uranium intermetallic compounds of composition UTX, where T is a transition-metal element and X is a p-electron metal, have been studied[1–4] with the intent to understand the role of $5f$-d hybridization in U-moment formation. Moving across the Periodic Table towards the end of the transition-metal series, the $5f$-d hybridization is generally reduced, allowing U-moment formation and magnetic ordering. In almost all ternary uranium intermetallic compounds, it has been found that the U moments are systematically aligned perpendicular to the directions of nearest-neighbor U-U links. The physical rationale for this is that the uranium $5f$ electrons are strongly hybridized in these directions. This leads to a compression of the $5f$ charge towards the U-U links. The associated orbital moment is then oriented perpendicular to these links. Such arguments have been shown to apply quantitatively in cubic Ce compounds.[5]

Recently, a large number of compounds of comparison U_2T_2X crystallizing in tetragonal U_3Si_2 structure has been studied.[6–8] The first reported[9] member of this group was U_2Co_2Al. The nearest U-U distance for most of them is along the c axis. Based on the phenomenological approach above, we expect the U moment to lie in the tetragonal basal plane; i.e., they have in-plane anisotropy. Two compounds, namely U_2Ni_2Sn and U_2Pd_2Sn, were reported to have nearest U-U neighbors in the basal plane rather than along the c axis. U_2Pd_2Sn is more critical in a sense that the difference between the nearest U-U distance and the next-nearest U-U distance, which is c, is much smaller than that of U_2Ni_2Sn.[6]

In this paper, we report results on two compounds: U_2Pd_2In and U_2Pd_2Sn, studied by bulk techniques and neutron diffraction.

II. METHODS

Polycrystalline samples were prepared by arc melting stoichiometric amounts of constituents of at least 99.99% purity. The phase purity was checked by a powder x-ray diffraction, which indicated a single-phase character of U_2Pd_2In. In the U_2Pd_2Sn sample a small amount (5–10 %) of an unidentified phase was detected. Therefore, the large sample of U_2Pd_2Sn for neutron diffraction (about 25 g) was annealed in a W crucible sealed under vacuum. The 10-day treatment at about 850 °C reduced the amount of the extra phase to the detectability limit of x-ray diffraction. Nevertheless, a very small amount of an unidentified extra phase was still visible in the neutron-diffraction patterns.

The crystal structure of both compounds was studied at room temperature using a four-circle x-ray diffractometer with graphite monochromated Mo-K_α ($\lambda=0.7107$ Å) radiation. For this study, small single-crystalline pieces were obtained by mechanical fragmentation of the cast material. Intensity data were collected in one octant of reciprocal space in the ω-2θ scan mode. The structure refinement was carried out on a Microvax

 ©1994 The American Physical Society

II computer using the Enraf-Nonius SPD program system.

The temperature dependence of the magnetic susceptibility was measured in fields up to 5 T in an Oxford Instruments Faraday balance system (U_2Pd_2Sn) and in a Quantum Design SQUID susceptometer (U_2Pd_2In). To prevent the influence of texture in the cast material, we studied samples in the form of powder fixed in a random orientation by a glue. We have also pursued magnetization studies at 4.2 K in high magnetic fields using the High Field Installation of the University of Amsterdam. This equipment allows measurement of magnetization in a quasistatic regime, in which the field is kept constant for about 0.1 s. Alternatively, one can measure magnetization during continuous field sweeps up and down. Two types of powder sample consisting of grains smaller than 100 μm were investigated. First, the particles are free to be oriented by the applied field, and second, they are fixed in a random orientation by frozen alcohol. In most cases, the free-powder experiment is thought to represent a measurement on a single crystal along the easy magnetization direction, whereas the fixed powder represents an "ideal" polycrystal. Consequently, the value of the free powder magnetization M_{free} is usually larger than the magnetization M_{fixed} of the fixed powder. By comparing both results, information about the type of magnetocrystalline anisotropy can be obtained. A standard ac four-probe method was used for resistivity measurements. Specific heat was measured down to 1.2 K in fields between 0 and 5 T by a semiadiabatic method.

For neutron-diffraction experiments, the samples were ground and enclosed with helium gas in sealed vanadium tubes which were mounted on the cold finger of a computer-controlled closed-cycle helium refrigerator. This, in turn, was installed on the High Intensity Powder Diffractometer[10] (HIPD) at the Los Alamos pulsed spallation neutron source LANSCE. HIPD currently has 8 banks of detectors at $2\theta = \pm 153°$, $\pm 90°$, $\pm 40°$, and $\pm 14°$. Data were taken at 50, 25, and 10 K for U_2Pd_2In and 50, 38, 35, and 10 K for U_2Pd_2Sn. The diffraction patterns were analyzed using the Rietveld refinement program GSAS which can refine the magnetic structure along with the crystallographic structure.[11] The magnetic intensities were also analyzed by extracting integrated intensities for individual peaks and fitting to models for the magnetic structures.

III. EXPERIMENTAL RESULTS

A. Crystal structure

U_2Pd_2X, where X can either be In or Sn, crystallizes in the tetragonal U_3Si_2-type structure[12] (space group $P4/mbm$). The uranium atoms occupy the $4h$ positions, palladium the $4g$, and the X atoms the $2a$ sites. A schematic view of the structure and a projection onto tetragonal basal plane is shown in Fig. 1. As seen from Fig. 1(a), the structure consists of two alternating types of basal plane sheets separated by $c/2$, one containing only the U atoms, the other accommodating Pd and X atoms. Its projection onto the tetragonal basal plane is shown in Fig. 1(b). Note that each uranium atom lies at the intersection of two mirror planes, one perpendicular to the c axis and the other shown by the dot-dashed line. The refined structural parameters, obtained from the x-ray-diffraction pattern taken at room temperature and from neutron diffraction at 50 K (the highest temperature at which the neutron experiments were performed), are listed in Table I.

The nearest U-U distances along the c axis ($d_\perp = c$) and in the a-b plane ($d_\parallel = 2\sqrt{2}ax_U$) are shown in Figs. 1(a) and 1(b), respectively. $d_\parallel$ is greater than $d_\perp$ at all temperatures measured for U_2Pd_2In, but in U_2Pd_2Sn, they are almost identical. For U_2Pd_2Sn, the temperature dependences of $d_\parallel$ and $d_\perp$ are shown in Fig. 2(a). At high temperature the nearest interuranium distance is $d_\parallel$. However, a crossover occurs at about 225 K and at low temperature, the nearest interuranium distance is $d_\perp$. In principle, the crossover could be due either to an anisotropic thermal contraction or to a change of U position (x_U) within the cell, or to a combination of the two.

Figure 2(b) shows three different curves as a function of temperature for U_2Pd_2Sn. One of them is the T depen-

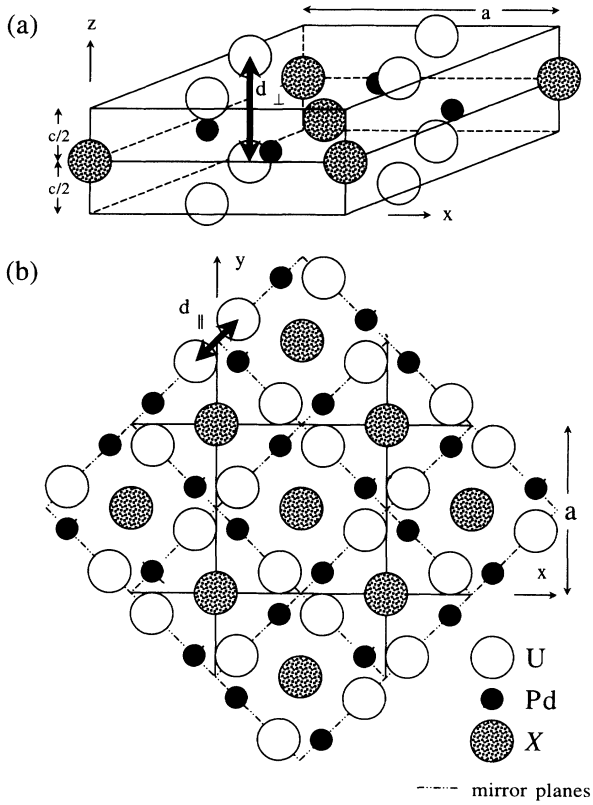

FIG. 1. The crystallographic structure of U_2Pd_2X, with X=In and Sn: (a) schematic view, showing the nearest U-U distance in c direction $d_\perp = c$ and (b) projected onto a plane perpendicular to the c axis, showing the nearest U-U distance in tetragonal basal plane $d_\parallel = 2\sqrt{2}ax_U$. The atom sizes are not drawn to scale, but the atom coordinates within the cell are drawn to scale.

TABLE I. Refined structural parameters for U_2Pd_2In and U_2Pd_2Sn at 50 K (neutron) and 300 K (x-ray).

				U_2Pd_2In	U_2Pd_2Sn
Space group $P4/mbm$					
U($4h$)	x_U,	$x_U+\frac{1}{2}$,	$\frac{1}{2}$	$x_U=0.174\,536\pm0.000\,031$ (50 K)	$0.176\,561\pm0.000\,036$ (50 K)
				$0.174\,38\pm0.000\,034$ (300 K)	$0.175\,67\pm0.000\,45$ (300 K)
Pd($4g$)	x_{Pd},	$x_{Pd}+\frac{1}{2}$,	0	$x_{Pd}=0.371\,323\pm0.000\,044$ (50 K)	$0.373\,159\pm0.000\,048$ (50 K)
				$0.371\,57\pm0.000\,75$ (300 K)	$0.372\,58\pm0.001\,04$ (300 K)
X($2a$)	0,	0,	0		
Lattice parameters				a(Å)$=7.623\,15\pm0.000\,32$ (50 K)	$7.588\,56\pm0.000\,27$ (50 K)
				7.637 ± 0.003 (300 K)	7.603 ± 0.002 (300 K)
				c(Å)$=3.739\,34\pm0.000\,16$ (50 K)	$3.771\,73\pm0.000\,14$ (50 K)
				3.752 ± 0.001 (300 K)	3.785 ± 0.001 (300 K)
R factors for 6 histograms (50 K)				$R_{wp}=4.72\%$	6.35%
				$R_p=3.24\%$	4.20%
				Reduced $\chi^2=5.467$	9.796

dence of $d_\perp$ and the other two are $d_\parallel(x_U)=(2\sqrt{2}\bar{a}x_U)$ and $d_\parallel(a)=(2\sqrt{2}a\bar{x}_U)$, where $\bar{a}$ and $\bar{x}$ are the mean values of a and x, respectively. Clearly, the crossover occurs between $d_\perp$ and $d_\parallel(x_U)$, not between $d_\perp$ and $d_\parallel(a)$. The expansion of $d_\parallel$ as the temperature is reduced is therefore due to temperature variation of U positions within the cell and not to anisotropic thermal contraction.

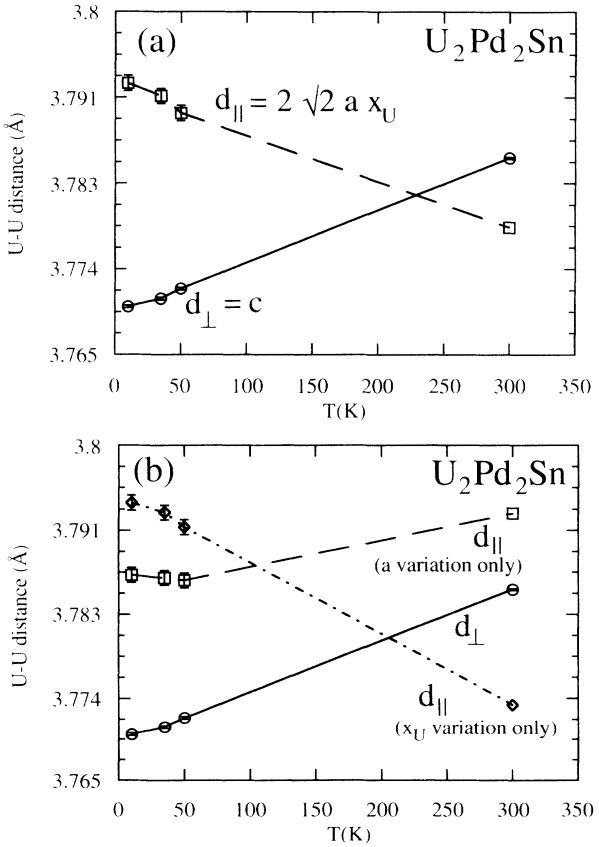

FIG. 2. Temperature dependence of the nearest uranium-uranium distance: (a) perpendicular $d_\perp$ (○) and in tetragonal basal plane $d_\parallel$ (□) for U_2Pd_2Sn. The two curves cross each other at about 225 K. (b) $d_\perp$ (○) is plotted again, along with suitably scaled variations of a (□) and x_U (◇). This figure shows definitively that the temperature variation of x_U is responsible for the anomalous behavior of $d_\parallel$.

B. Magnetic properties

1. *Bulk measurements*

(a) Magnetic susceptibility and magnetization. The temperature dependence of the magnetic susceptibility χ of U_2Pd_2In was measured at 0.1, 1, 2, and 4 T. Since there is almost no field dependence of χ, we display in Fig. 3(a) only results obtained in 4 T. The characteristic maximum of χ, marking the onset of antiferromagnetic ordering, occurs just below 40 K. In the low-temperature limit, χ decreases to about 15.7×10^{-8} $m^3/mol_{f.u.}$.

In the paramagnetic range, the $\chi(T)$ data follow approximately Curie-Weiss (CW) behavior:

$$\chi=C/(T-\Theta_p)\,. \tag{1}$$

Equation (1) fits the data well above 100 K, with paramagnetic Curie temperature $\Theta_p=-83$ K and Curie constant $C=3.1\times10^{-5}$ m^3 K/$mol_{f.u.}$ yielding an effective moment $\mu_{eff}=3.1\mu_B$/U atom. Assuming a modified Curie-Weiss (MCW) law,

$$\chi=C/(T-\Theta_p)+\chi_0\,, \tag{2}$$

containing the temperature-independent term χ_0, a more reasonable fit is achieved in the range 70–330 K. Now the fitting parameters are $C=2.02\times10^{-5}$ m^3 K/$mol_{f.u.}$ ($\mu_{eff}=2.1$ μ_B/U atom), $\theta_p=-32.3$ K, and $\chi_0=1.9\times10^{-8}$ $m^3/mol_{f.u.}$. Nevertheless, the success of the MCW fit does not necessarily mean the presence of a temperature-independent contribution. Experience shows that very similar behavior can be due to a polycrystalline averaging in anisotropic compounds of several CW branches differing, for example, in the Θ_p value.

U_2Pd_2Sn displays qualitatively similar behavior [see Fig. 3(b)]. The susceptibility maximum is found at about 43 K and at low temperatures χ decreases to about 12×10^{-8} $m^3/mol_{f.u.}$. A closer inspection of the paramagnetic range shows that, unlike U_2Pd_2In, the Sn compound follows a Curie-Weiss behavior (1) over the temperature range 60–200 K. In this range, we obtain

$\mu_{eff}=2.83\ \mu_B/U$ and $\Theta_p=-50$ K. By the high-temperature end (above 240 K), the $\chi(T)$ dependence tends to larger values of μ_{eff} (about $3.1\mu_B/U$) and to $\Theta_p\approx-100$ K. Alternatively, one can also use the MCW law (2), which accounts for the $\chi(T)$ dependence at temperatures above 120 K. The fitting parameters are $C=1.94\times10^{-5}$ m^3 K/$mol_{f.u.}$ ($\mu_{eff}=2.5\mu_B/U$), $\chi_0=1.4\times10^{-8}$ $m^3/mol_{f.u.}$, and $\Theta_p=-30.3$ K. Below 60 K, the $\chi(T)$ dependence levels out and the Néel temperature is manifest as a drop of χ at 41 K.

Complementary information on the magnetic state can be obtained from high-field magnetization studies. Figure 4 shows such data from both compounds up to 38 T. In U_2Pd_2In, there is a clear evidence of a field-induced transition at 25 T. For powder frozen in alcohol, the magnetization above the transition continues to increase with magnetic field (showing only a slow saturation tendency) yielding 0.83 μ_B/U in 38 T. This value is still far from the saturation magnetization of 1.45 μ_B/U estimated from the linear extrapolation of M vs $1/B$ plot to $1/B=0$. The metamagnetic transition is also manifest in the free-powder measurement, but surprisingly the increment of M in the transition is much reduced and only $0.63\mu_B/U$ is attained in 38 T. The fact that the free-powder magnetization is smaller in fields above the transition is rather exceptional and may be understood if the easy magnetization direction (direction of the largest susceptibility) in fields below 25 T is perpendicular to that in which the metamagnetic transition can be induced around 25 T. The lower fields (where, indeed, $M_{free}>M_{fixed}$) orient powder grains with the latter direction perpendicular to the magnetic field. Then the metamagnetic transition cannot be achieved and the spurious effect on the magnetization curve above 25 T is due to certain amount of grains poorly oriented in low fields. To solve this puzzle, single-crystal magnetization data are strongly desired, but we can conclude that U_2Pd_2In does not have strong uniaxial anisotropy.

For U_2Pd_2Sn, no such clear transition is achieved in

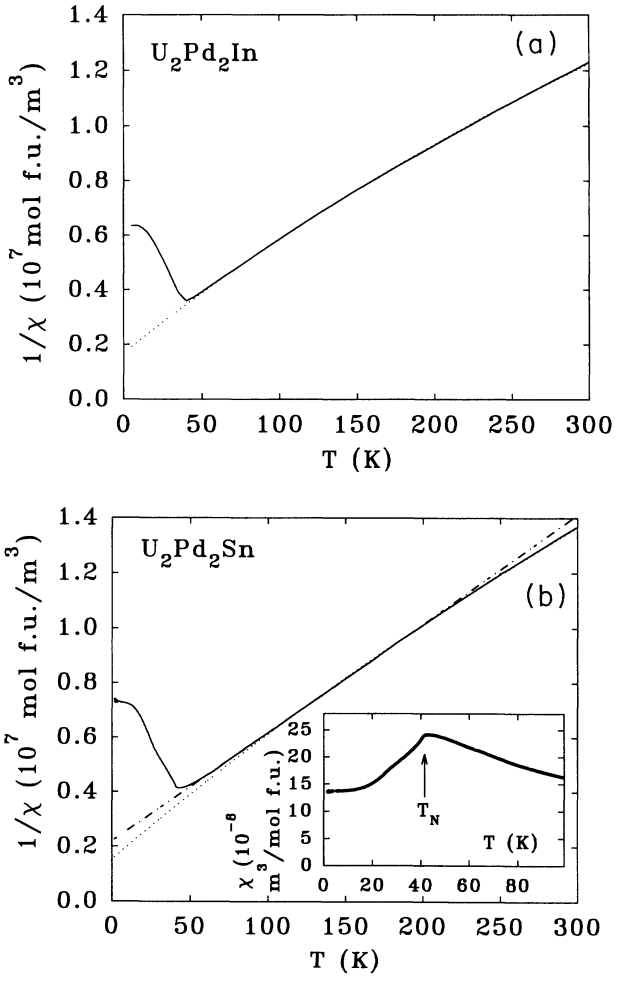

FIG. 3. Temperature dependence of the inverse susceptibility of (a) U_2Pd_2In and (b) U_2Pd_2Sn. The dotted lines represent the fits to the modified Curie-Weiss law [see Eq. (2)] and the dot-dashed line in (b) a fit to the Curie-Weiss law [see Eq. (1)] with parameters described in text. For (b), the inset shows the low-temperature part of $\chi(T)$ with arrow indicating the Néel temperature.

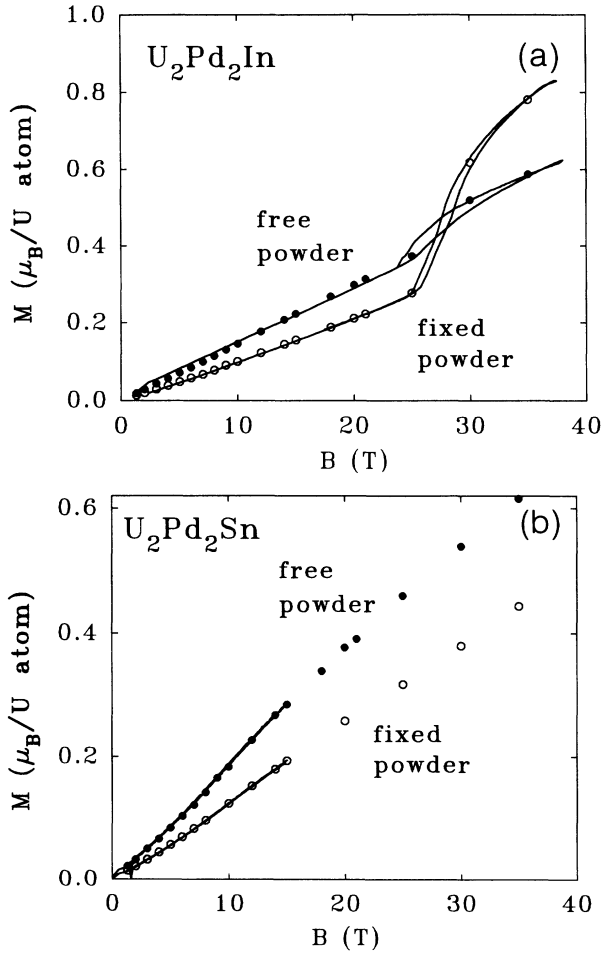

FIG. 4. Magnetization curves of (a) U_2Pd_2In and (b) U_2Pd_2Sn at 4.2 K measured on free powder (●) and fixed powder (○) samples. The solid lines represent the continuous-field-sweep measurements, which show noticeable hysteresis around the metamagnetic transition for U_2Pd_2In.

the available fields. Both $M(B)$ branches are approximately linear and similar to those measured in the U_2Pd_2In sample in fields below 25 T. However, a close inspection shows that the free-powder branch displays a weak S shape with inflection point at about 10 T. In this case, conclusions on the nature of the magnetization process also require single-crystal experiments.

(b) Specific heat. The specific heat of U_2Pd_2In, displayed in Fig. 5, is dominated by a pronounced anomaly at 36 K (connected with the paramagnetic-antiferromagnetic phase transition): as usual, this temperature is somewhat lower than the temperature of the susceptibility maximum.[13] In the range above 55 K, the specific heat can be well described by Debye model for the lattice specific heat with a Debye temperature $\Theta_D = 185$ K, assuming a linear coefficient of the electronic specific heat $\gamma_0 = 65$ mJ/mol$_{\text{f.u.}}$ K^2. The effect of a magnetic field of 5 T on the temperature dependence of the specific heat is almost negligible. This applies also to the low-temperature upturn, shown in Fig. 6, indicating that it is intrinsic.

We have tried to check whether the upturn can be described by an additional logarithmic term, which can be attributed, for example, to spin fluctuations (paramagnons),[14] $C_{\text{sf}} = \delta T^3 \ln T$. In this context, we found that a reasonable agreement with experimental data over a significant temperature range can only be obtained if we also consider a magnon contribution $C_{\text{magnon}} = \alpha T^{1/2} \exp(-\Delta/T)$. This describes the magnetic excitations across an anisotropic gap Δ in the magnon spectrum.[15] Thus, we have fitted the low-temperature (up to 15 K) experimental data to the expression

$$C = \gamma T + \beta^* T^3 + \delta T^3 \ln T + \alpha T^{1/2} \exp(-\Delta/T) \quad (3)$$

with the parameters $\gamma = 0.393$ J/mol$_{\text{f.u.}}$ K^2, $\beta^* = -0.0055$ J/mol$_{\text{f.u.}}$ K^4, $\delta = 0.002\,11$ J/mol$_{\text{f.u.}}$ K^4, $\alpha = 7.405$ J/mol$_{\text{f.u.}}$ K$^{3/2}$, and $\Delta = 27$ K. The presence of magnonlike excitations with moderate Δ can indeed be considered in a system of planar type of anisotropy. We assume the functional form

$$\beta^* = \beta - \delta \ln T_{\text{sf}} , \quad (4)$$

where $\beta = 0.0015$ J/mol$_{\text{f.u.}}$ K^4 describes the low-temperature part of the Debye function extracted from C vs T in the paramagnetic range. The characteristic temperature of spin fluctuations T_{sf} is approximately 30 K. The magnetic entropy obtained as

$$S_m = \int_0^{50\text{ K}} (C/T - C_{\text{Debye}}/T) dT \quad (5)$$

and normalized to 1 mol of U gives about $1.1R$ ln2.

In U_2Pd_2Sn, the magnetic phase transition shows up as a pronounced maximum at $T = 41.2$ K, and the maximum shifts to slightly lower temperatures (by about 0.2 K) in $B = 5$ T. Note that the different character of the maximum in U_2Pd_2In, which points to a different critical behavior, does not allow a comparable resolution in the determination of T_N and, therefore, we cannot exclude a similar shift in external fields. The high-temperature part can be described by a Debye function assuming $\Theta_D = 212$ K. The other assumption, $\gamma_0 = 0$, is somewhat unrealistic for a metallic specimen. Nevertheless, we tried to use such a background function to estimate the magnetic entropy using expression (5). Integrating up to 80 K, where $C/T - C_{\text{Debye}}/T$ goes to 0, we obtain a magnetic entropy of about $2R$ ln2. This should be understood as an upper limit, because the actual $\gamma = 203$ mJ/mol$_{\text{f.u.}}$ K^2 is significantly higher than γ_0.

The difference between $\gamma = (C/T)_{T \to 0}$ and γ_0, obtained by extrapolation from the paramagnetic range, can normally be attributed to variations of $N(E_F)$, the density of electronic states at the Fermi level. However, the magnetic ordering is normally expected to remove part of the single-particle electron density of states from E_F, which leads to a decrease of the electronic contribution to C in

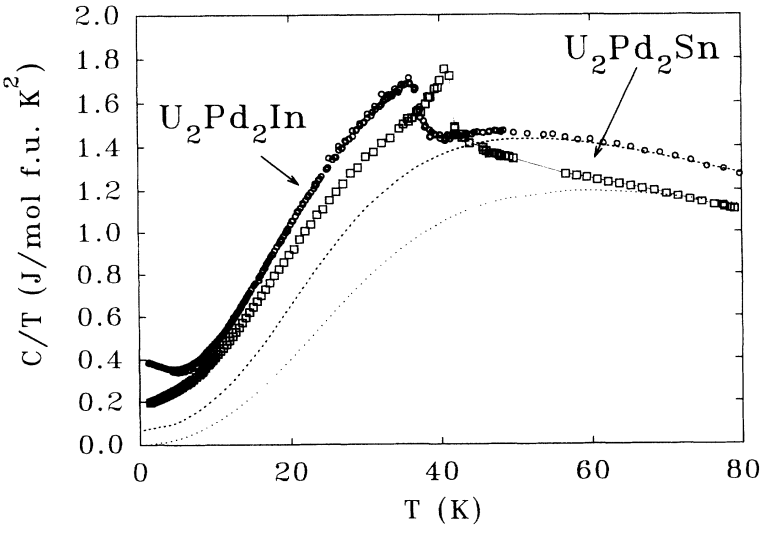

FIG. 5. Temperature dependence of the specific heat of U_2Pd_2In (○) and U_2Pd_2Sn (□) in zero field, presented in the form of C/T vs T plots. The dotted and dashed curves represent the Debye specific heat of U_2Pd_2In and U_2Pd_2Sn, respectively.

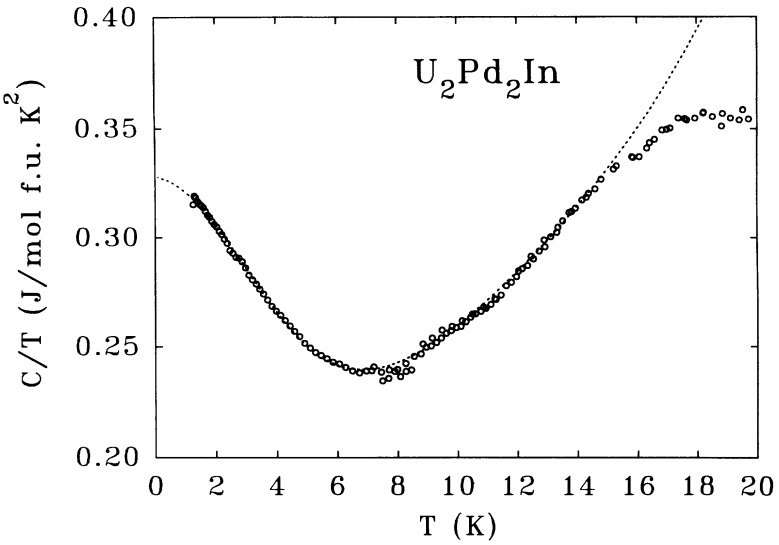

FIG. 6. The low-temperature detail of the C/T vs T plot for U_2Pd_2In in zero field. The dotted curve represents the fit according to Eq. (3) described in text. The Debye function determined from the high-temperature part was subtracted.

the ordered state. Alternatively, one can think of variations of the lattice contribution to C or of a quasiparticle spectrum in the ordered state leading to $\gamma > \gamma_0$. In any case, such a situation makes any subtraction of the lattice contribution more speculative. Attempting to perform a lower limit for the entropy estimate, we can calculate the same expression upon lifting C_{Debye}/T up by the γ value of 0.203 J/mol$_{\text{f.u.}}$ K^2, which yields $0.95R$ ln2. Assuming such a background, we can also analyze terms in expression (3), in which the logarithmic term can be neglected due to the absence of any low-temperature upturn. The fitting results in $\alpha = 4.9$ J/mol$_{\text{f.u.}}$ K$^{3/2}$ and $\Delta = 27$ K, and the fit describes the data well up to about 30 K.

The upper limits of integration in expression (5) are higher than the corresponding values of T_N. The reason is that a considerable portion of magnetic entropy lies above T_N, as seen from Fig. 5. This effect, which can be attributed to short-range order in the paramagnetic state, is more pronounced in U_2Pd_2Sn. It is also qualitatively consistent with a stronger departure from the CW behavior of susceptibility in this compound.

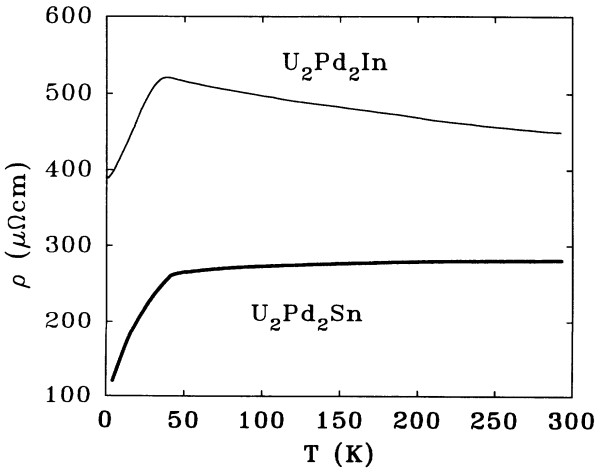

FIG. 7. Temperature dependence of the resistivity of U_2Pd_2In and U_2Pd_2Sn.

(c) Electrical resistivity. Electrical resistivity was measured on bar-shaped samples cut from the cast button. Due to the possible influence of anisotropy in materials with a cast texture, the data should be interpreted with caution. Although both materials reveal anomalies at their Néel temperatures, their behavior is qualitatively different, especially at high temperatures. Figure 7 shows the temperature dependence of ρ in U_2Pd_2In and U_2Pd_2Sn. The high-temperature $\rho(T)$ curve for U_2Pd_2Sn is quite flat above T_N and tends progressively to saturation with $d\rho/dT$ remaining positive. For U_2Pd_2In, we observe a larger and negative slope. The uncertainty in absolute values of ρ is largely due to internal cracks, so we are unsure how significant the difference between the two compounds is. But the order of magnitude of hundreds of $\mu\Omega$ cm is rather standard in narrow $5f$-band materials.

The temperature range studied first (down to 5 K) does not allow us to observe the saturation of $\rho(T)$ in the low-temperature limit. Therefore, for U_2Pd_2In, we extended the range down to 150 mK. Surprisingly, no quadratic $\rho(T)$ dependence could be found. Instead, the initial increase of ρ is much slower and can be described by the power law:

$$\rho = \rho_0 + aT^n \tag{6}$$

with $\rho_0 = 387.8\,\mu\Omega$ cm, $a = 1.47\,\mu\Omega$ cm K^{-n}, and $n = 1.36$.

2. Neutron diffraction

Figure 8 shows some of the raw data from U_2Pd_2In taken in the $+90°$ bank of HIPD at two temperatures (10 and 25 K) below T_N and one temperature (50 K) above T_N. The bottom plot is a difference curve between the 10- and 50-K raw data for the $+90°$ bank combined with the $-90°$ bank. Figure 9 shows some of raw data of U_2Pd_2In taken in the $+153°$ bank of HIPD at three temperatures (10, 35, and 38 K) below T_N and one tempera-

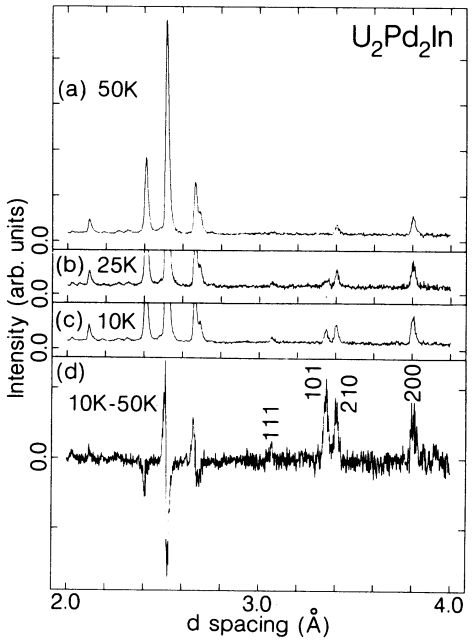

FIG. 8. Plot of a portion of the U_2Pd_2In raw neutron-diffraction data taken in the $+90°$ bank of HIPD at three temperatures: (a) at 50 K, (b) at 25 K, (c) at 10 K. As the temperature is lowered, an extra peak appears at about 3.35 Å, indexed as (101) in tetragonal symmetry. The bottom plot (d) is the 10–50 K difference curve. The intensities have been divided by the incident spectrum.

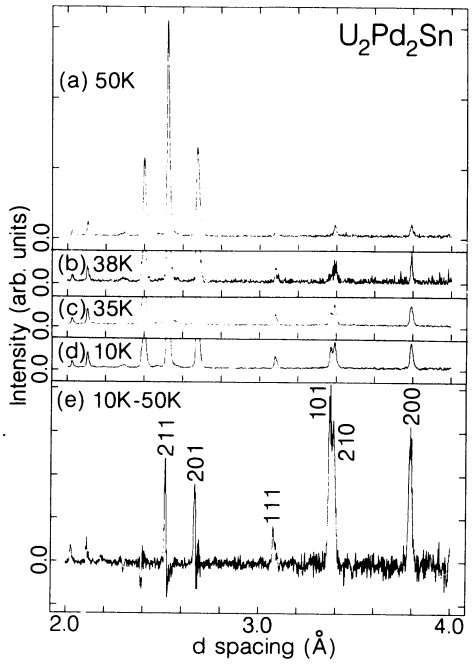

FIG. 9. Plot of a portion of the U_2Pd_2Sn raw neutron-diffraction data taken at the $+153°$ bank of HIPD at four temperatures: (a) at 50 K, (b) at 38 K, (c) at 35 K, and (d) at 10 K. As the temperature lowers, an extra peak appears at about 3.37 A, indexed as 101 in tetragonal symmetry. Note that the beam time of the 38-K data is only 10% of the 50-K data. The bottom plot (e) is the 10–50 K difference curve. The intensities have been divided by the incident spectrum.

ture (50 K) above T_N. The bottom plot is a difference curve between the 10- and 50-K raw data for the $+153°$ bank combined with the $-153°$ bank. As shown in Figs. 8 and 9, a pure magnetic contribution appears as an extra peak below T_N at about 3.4 Å for both compounds. This extra magnetic peak is indexable as (101) in the tetragonal cell, and we assume that the magnetic cell is the same as the nuclear one.

Apart from this extra peak, there are some peaks with higher observed intensities below T_N and we also attribute these increases to magnetic ordering. Those peaks are (111), (210), (200) for both compounds and in addition (201), (211) for U_2Pd_2Sn. Figure 10 shows some of raw data taken in the $+40°$ bank at 10 K for both compounds. Clearly, there is no (100) reflection, which would occur at about 7.6 Å.

First, let us consider possible *collinear* models of magnetic moment arrangement. There are only two independent antiferromagnetic configurations $C1$ and $C2$, as shown in Figs. 11(a) and 11(b). The interference part of the cross section (ignoring magnetic form factor, Lorentz factor, and so on) can be written as[16]

$$I_{C1} \propto \begin{cases} \{4\sin\eta \sin(2\pi x_U k)\cos(2\pi x_U h)\}^2 & \text{for } (h+k) \text{ odd}, \\ \{4\sin\eta \sin(2\pi x_U h)\cos(2\pi x_U k)\}^2 & \text{for } (h+k) \text{ even}, \end{cases} \tag{7}$$

$$I_{C2} \propto \begin{cases} \{4\sin\eta \cos(2\pi x_U h)\cos(2\pi x_U k)\}^2 & \text{for } (h+k) \text{ odd}, \\ \{4\sin\eta \sin(2\pi x_U h)\sin(2\pi x_U k)\}^2 & \text{for } (h+k) \text{ even}, \end{cases} \tag{8}$$

where η is the angle between the moment direction and the reciprocal lattice vector for the corresponding Bragg reflection. The subscripts $C1$ and $C2$ correspond to the models represented by Figs. 11(a) and 11(b), respectively. Note that there is no third Miller index (l) dependence, as all four uranium atoms lie at $z=\frac{1}{2}$. Clearly, all $10l$ reflections (including 100 reflection) have nonzero intensities for both models. However, as shown in Fig. 11, there is no observed (100) reflection. Hence, the collinear antiferromagnetic models do not apply.

Now, let us consider possible *noncollinear* structures using the magnetic space group formalism.[17] There are six independent Shubnikov subgroups of $P4/mbm$ as shown in Fig. 12. Two are collinear subgroups and four

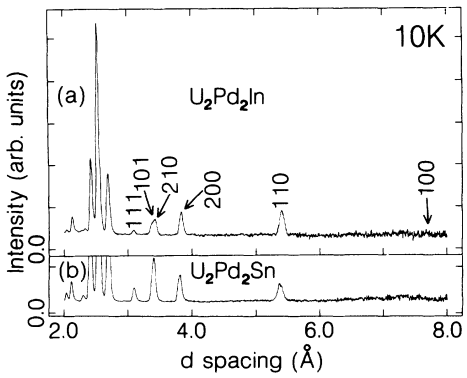

FIG. 10. Plot of a portion of the (a) U_2Pd_2In and (b) U_2Pd_2Sn raw neutron-diffraction data taken at the +40° bank of HIPD at 10 K. Note that the (100) reflection is absent.

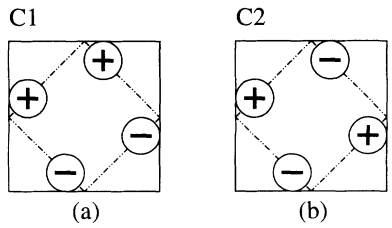

FIG. 11. The two possible collinear antiferromagnetic models, $C1$ and $C2$, projected onto the tetragonal basal plane. Only the U atoms are shown, represented by circles with +'s and −'s denoting the relative moment directions between each other. The dashed lines represent the mirror planes. The atom sizes are not drawn to scale, but the atom coordinates within the cell are drawn to scale. These figures correspond to the central square in Fig. 1(b).

are noncollinear ones. In the collinear models, moments are in the c direction while the moments lie in the basal plane in all four noncollinear models. The collinear ferromagnetic model does not give the (101) reflection: the selection rule of the ferromagnetic model is just that of the nuclear structure. The collinear antiferromagnetic model was considered previously (model $C2$ in Fig. 11) and eliminated. Two of the noncollinear models ($NC2$ and $NC4$) with the structure shown in Figs. 12(d) and 12(f) have calculated intensity at the (100) reflection which is not observed in the diffraction pattern. The other noncollinear model ($NC3$) represented by Fig. 12(e) gives intensity in all observed magnetic peaks but too much calculated intensity at (110) and too little at (101) and (201). Finally, the magnetic structure ($NC1$) represented by Fig. 12(c) gives a good fit to the intensities in all observed reflections. For the five possible antiferromagnetic models (AFC, $NC1$, $NC2$, $NC3$, $NC4$), R factors and goodnesses of fit for both compounds at 10 K are shown in Table II. Clearly the noncollinear model $NC1$ gives the best fit to the data and we obtain U-moment magnitudes of $(1.40\pm0.02)\mu_B$ and $(1.89\pm0.01)\mu_B$ for U_2Pd_2In and U_2Pd_2Sn, respectively. As a check, the traditional method of fitting integrated intensities from individual reflections to the magnetic model was used for all four noncollinear models and both collinear antiferromagnetic models ($C1$ and $C2$ shown in Fig. 11). Note that the $C1$ model does not have tetragonal symmetry. The integrated nuclear and magnetic intensities of (200), (210), (101), (111), (100) for both compounds and in addition (201), (211) for U_2Pd_2Sn were extracted using the program FIT_PEAKS.[18] The calculated intensities include the U form factor[19] and the Lorentz factor. The result is shown in Table III and again the noncollinear model $NC1$ gives the best fit to the data. We obtain the U-moment magnitudes of $(1.73\pm0.01)\mu_B$ and $(2.00\pm0.01)\mu_B$ for U_2Pd_2In and U_2Pd_2Sn, respectively. These error bars are obtained solely by propagating statistical errors. The discrepancies between the two methods of analysis indicate that there are systematic errors of $0.1-0.2\mu_B$, which is typical of magnetic powder diffraction experiments.

IV. DISCUSSION

The main result of this work is that these two compounds conform to the same phenomenological picture as the (1:1:1) uranium ternary intermetallics, in which the U moments almost invariably lie perpendicular to nearest-neighbor U-U links, whether they form chains or planes. In the present case, the nearest-neighbor links are along the tetragonal c axis, and the magnetic anisotropy is of a planar type, with the moments forming a noncollinear arrangement in the tetragonal basal plane. If the ideas of

TABLE II. R factors and reduced χ^2 for U_2Pd_2In and U_2Pd_2Sn at 10 K using Rietveld refinement program GSAS (Ref. 11).

Model	U_2Pd_2In			U_2Pd_2Sn		
	wRp (%)	Rp (%)	Reduced χ^2	wRp (%)	Rp (%)	Reduced χ^2
AFC	4.93	3.49	5.00	5.67	3.91	12.16
$NC1$	4.61	3.23	4.38	4.94	3.50	9.23
$NC2$	4.91	3.46	4.96	5.68	3.91	12.18
$NC3$	4.83	3.40	4.80	5.25	3.56	10.40
$NC4$	4.91	3.47	4.97	5.67	3.90	12.16

TABLE III. Reduced χ^2 for U_2Pd_2In and U_2Pd_2Sn at 10 K fitting to individual integrated intensities.

Model	U_2Pd_2In	U_2Pd_2Sn
$C1$	4.81	4.07
$C2$	14.99	13.62
AFC	14.99	13.62
$NC1$	4.59	2.96
$NC2$	14.99	13.62
$NC3$	7.70	6.30
$NC4$	14.99	13.62

hybridization-induced anisotropy, developed for cubic Ce compounds, and applied more recently to U compounds work here, we would state that the hybridization is stronger along the c axis. This would result in ferromagnetic exchange along the c direction, which we observe. We note that, while U_2Pd_2In clearly has nearest U-U neighbors along the c axis, the other compound, U_2Pd_2Sn, is very close to the borderline of having U-U links in the basal plane. For U_2Pd_2Sn, our crystallographic data indicate a crossover of the two nearest-neighbor distances $d_\perp = c$ and $d_\parallel = 2\sqrt{2}ax_U$ with temperature. A possible impact on the $\chi(T)$ dependence of such crossover, which is expected at about 225 K, can, in principle, be traced out from the experimental data, but single-crystal data are needed for a more conclusive analysis.

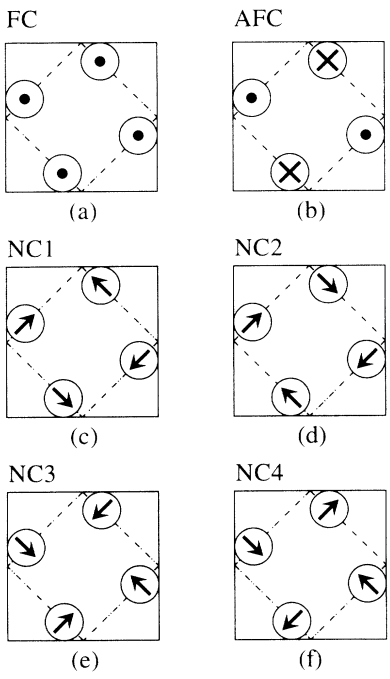

FIG. 12. Projections on the tetragonal basal plane of two collinear Shubnikov subgroups: (a) c-axis ferromagnetic FC, (b) c-axis antiferromagnet AFC, and four noncollinear Shubnikov subgroups: (c) $NC1$, (d) $NC2$, (e) $NC3$, (f) $NC4$; for the $4h$ site in $P4/mbm$. Only the U atoms are shown, represented by circles. The moments are symbolized by dots if out of the plane of paper, crosses for moments into the plane of paper. The dashed lines represent mirror planes. The atom sizes are not drawn to scale, but the atom coordinates within the cell are drawn to scale. These figures correspond to the central square in Fig. 1(b).

A second consideration is that, of the two compounds reported here, U_2Pd_2Sn seems to be more localized in character than U_2Pd_2In, as its ordered moment is larger. It seems that the stronger delocalization of In compounds of the 2:2:1 type with respect to the Sn counterparts is a general feature. It is most conspicuous comparing U_2Rh_2In and U_2Pt_2In (nonmagnetic) with U_2Rh_2Sn and U_2Pt_2Sn (magnetic).[20] We note that for U_2Pd_2In, the ordered moment obtained by extrapolating high-field magnetization data ($1.5\mu_B$) is also slightly lower than that obtained by neutron scattering ($1.6\mu_B$).

Another argument indicating the stronger delocalization of the $5f$ states in U_2Pd_2In is the higher γ coefficient of the low-temperature specific heat compared to that in U_2Pd_2Sn. Although the origin of strongly enhanced γ's in most 2:2:1 compounds is not yet clear, it seems that the γ enhancement scales systematically with proximity to the onset of magnetic ordering. It reaches a maximum (about 800 $mJ/mol_{f.u.}\,K^2$), in nearly magnetic U_2Pt_2In.[20] The systematic occurrence of numerous compounds with such a strong γ enhancement (most of them can be classified as heavy fermions) makes the group of 2:2:1 compounds exceptional among uranium intermetallics.

Magnetic symmetry arguments apply well to the magnetic structures in these two compounds. The U atoms lie at the intersection of two mirror planes, one parallel to the tetragonal basal plane and the second perpendicular to the [110] or [1$\bar{1}$0] axis, depending on the site, as shown by the dashed lines in Fig. 12. It is well known that magnetic atoms in mirror planes must have moments either purely within the plane, or purely perpendicular. In this case, these conditions must be met for both mirror planes simultaneously, as shown in Fig. 12; there are two structures with moments along the c axis, two with moments in plane, but lying in the (110)-type planes, and two with in-plane moments perpendicular to the (110)-type planes. Our data clearly prefer structure $NC1$, with moments lying in both mirror planes. Thus, the in-plane anisotropy must prefer moments with [110] directions in mirror planes. As for the interactions, the nearest-neighbor exchange (along the c axis) is ferromagnetic, while the next-nearest-neighbor exchange [along $d_\parallel$ as shown in Fig. 1(b)] is antiferromagnetic. Given that these are satisfied, the third-nearest-neighbor exchange gives no contribution to the internal energy, as the uranium moments form pairs with no net moment. Single-ion anisotropy will distinguish between models $NC3$ and $NC4$ on the one hand, and models $NC1$ and $NC2$ on the other. The fact that structure $NC1$ is observed indicates that the easy axis lies in both mirror planes. But even then, the energies of $NC1$ and $NC2$ are equal, if one includes only isotropic exchange and single-ion anisotropy. The Dzyaloshinskii-Moriya interaction[21] between the third-nearest neighbors can, however, distinguish between $NC1$ and $NC2$, depending on its sign. Another possibility is the classical dipole-dipole interaction between the third-

nearest neighbors, but it will prefer $NC2$ over $NC1$, in contrast to our observation.

In conclusion, we have determined the bulk magnetic properties, the magnetic transition temperatures, and the magnetic structures of U_2Pd_2In and U_2Pd_2Sn. We have shown that both have the same type of magnetic anisotropy, forcing U moments to orient perpendicular to the nearest U-U links. We have also demonstrated the existence of a metamagnetic transition in U_2Pd_2In at 25 T, but its character will probably only be elucidated when single crystals become available. U_2Pd_2In also displays a low-temperature upturn in C/T and enhanced γ of 393 $mJ/mol_{f.u.}\ K^2$, which indicates a $5f$ moment instability in contrast to U_2Pd_2Sn with γ of 203 $mJ/mol_{f.u.}\ K^2$ and larger U moments.

ACKNOWLEDGMENTS

We are grateful to D. Coffey and S. Trugman for helpful discussion regarding the free energy of these systems. This work was supported by the U.S.-Czechoslovak Science and Technology Joint Fund under Project No. 93039 and by the Grant Agency of Czech Republic (Grant No. 202/93/0184). It was also supported in part by the division of Basic Energy Sciences of the U.S. Department of Energy. Part of the work was also supported by the "Stichting voor Fundamenteel Onderzoek der Materie" (FOM). Support to A.S. and J.M.W. given in the frame of the E.C. funded training program Human Capital and Mobility is acknowledged. Part of the work of L.H. was done during his stay in I.T.U. Karlsruhe.

*Also Department of Physics, New Mexico State University, Las Cruces, NM 88003.

[1]R. A. Robinson, A. C. Lawson, V. Sechovský, L. Havela, Y. Kergadallan, H. Nakotte, and F. R. de Boer, J. Alloys Comp. (to be published).

[2]V. Sechovský and L. Havela, in *Ferromagnetic Materials-A Handbook on the Properties of Magnetically Ordered Substances,* edited by E. P. Wohlfarth and K. H. J. Buschow (North-Holland, Amsterdam, 1988), Vol. IV, pp. 309–491.

[3]V. Sechovský and L. Havela, J. Magn. Magn. Mater. **104-107**, 7 (1992).

[4]J. A. Paixão, G. H. Lander, P. J. Brown, H. Nakotte, F. R. de Boer, and E. Brück, J. Phys.: Condens. Matter **4**, 829 (1992).

[5]B. R. Cooper, R. Siemann, D. Yang, P. Thayamballi, and A. Banerjea, in *Handbook on the Physics and Chemistry of the Actinides,* edited by A. J. Freeman and G. H. Lander (North-Holland, Amsterdam, 1985), Vol. II, pp. 435–500.

[6]H. Nakotte, K. Prokeš, E. Brück, N. Tang, and F. R. de Boer, P. Svoboda, V. Sechovský, L. Havela, J. M. Winand, A. Seret, J. Rebizant, and J. C. Spirlet, Physica B (to be published).

[7]F. Mirambet, P. Gravereau, B. Chevalier, L. Trut, and J. Etourneau, J. Alloys Comp. **191**, L1 (1993).

[8]M. N. Peron, Y. Kergadallan, J. Rebizant, D. Meyer, J. M. Winand, S. Zwirner, L. Havela, H. Nakotte, J. C. Spirlet, G. M. Kalvius, E. Collineau, J. L. Oddou, C. Jeandey, and J. P. Sanchez, J. Alloys Comp. **201**, 203 (1993).

[9]A. O. Sampaio, E. Santa Marta, H. L. Lukas, and G. Petzow, J. Less-Common Met. **14**, 472 (1968).

[10]A. C. Lawson, J. A. Goldstone, J. G. Huber, A. L. Giorgi, J. W. Conant, A. Severing, B. Cort, and R. A. Robinson, J. Appl. Phys. **69**, 8 (1991).

[11]A. C. Larson and R. B. Von Dreele, Los Alamos National Laboratory Report No. LA-UR-86-748 (unpublished).

[12]W. Zachariasen, Acta Crystallogr. **2**, 94 (1949).

[13]The magnetic phase transition is better associated with the maximum in $\partial(\chi T)/\partial T$ as shown by M. E. Fischer, Philos. Mag. **7**, 1731 (1962); P. A. Fedders and P. C. Martin, Phys. Rev. **143**, 245 (1966).

[14]S. Doniach and S. Engelsberg, Phys. Rev. Lett. **17**, 750 (1966); W. F. Brinkman and S. Engelsberg, Phys. Rev. **169**, 417 (1968).

[15]N. Hessel Andersen and H. Smith, Phys. Rev. B **19**, 384 (1979).

[16]G. L. Squires, *Introduction to the Thermal Neutron Scattering* (Cambridge University Press, Cambridge, 1978), p. 150ff.

[17]W. Prandl, in *Neutron Diffraction,* edited by H. Dachs (Springer, Berlin, 1978), Chap. 4.

[18]J. A. Goldstone (private communication).

[19]S. W. Johnson, R. A. Robinson, H. Nakotte, E. Brück, F. R. de Boer, and A. C. Larson, J. Appl. Phys. **73**, 6072 (1993).

[20]L. Havela, V. Sechovský, P. Svoboda, M. Diviš, H. Nakotte, K. Prokeš, F. R. de Boer, A. Purwanto, R. A. Robinson, A. Seret, J. M. Winand, J. Rebizant, J. C. Spirlet, M. Richter, and H. Eschrig, *Proceedings of the 6th MMM-Intermag Conference,* Albuquerque, 1994 [J. Appl. Phys. (to be published)].

[21]D. Coffey, K. S. Bedell, and S. A. Trugman, Phys. Rev. B **42**, 6509 (1990).